# ASPL-APBT Algorithm for Block Compressed Sensing Image Reconstruction

Aiping Yang*, Gai Li, Zhengxing Hou, and Yuqing He
School of Electronic Information Engineering, Tianjin University, Tianjin 300072, P. R. China
Email: yangaiping@tju.edu.cn; ligai825@163.com; zhengxinhou@163.com; heyuqing@tju.edu.cn

***Abstract***—Based on the block compressed sensing (BCS) framework, a new and non-orthogonal transform named all phase biorthogonal transform (APBT) is introduced to exploit the image sparsity, reduce the encoding complexity and be applicable to the blocked image easily. APBT exploits the signal sparsity better than DCT, and meanwhile it overcomes the defects of multiscale transform such as wavelet transform with high computational complexity and the feature of not being applicable to the blocked image. In order to improve the efficiency of BCS reconstruction, the accelerated smoothed projected Landweber (ASPL) iteration algorithm is put forward. Combined with the sparse constraints in APBT, the BCS-ASPL-APBT reconstruction algorithm is advanced. Experimental results demonstrate that the proposed algorithm outperforms the method of using DCT sparsifying coupled with common SPL iteration not only in the aspect of PSNR, but in terms of the reconstruction time and the iteration number.

***Index Terms***—Block compressed sensing; APBT; SPL; accelerated SPL

## I. INTRODUCTION

Compressed sensing (CS) has gained increasing interests over the past few years. The CS theory demonstrates that signals with sparse representation under some transform domain can be precisely reconstructed only from a small set of measurements [1]-[3]. As applied to 2D images, however, CS faces several challenges including a computationally expensive reconstruction process and huge memory required to store the random sampling operator. Recently, several fast algorithms [4], [5] have been developed for CS reconstruction, but with the reconstruction quality as the sacrifice. With the purpose of resolving huge memory for sensing matrix, the structurally random sensing matrixes were addressed in [6], [7], but these matrixes have poor universality. So the block compressed sensing (BCS) theory was advanced in [8], [9], in which the block-based sampling operation was used and the smoothed projection-based Landweber iterations (SPL) was proposed to accomplish CS reconstruction aiming at improving the reconstructed-image quality by eliminating blocking artifacts. In recent years SPL based methods have been used extensively for CS reconstruction: Chen firstly used the spatial redundancy to make a prediction for the original image by the multi-hypothesis theory, and then applied SPL algorithm to reconstruct the residual between the original and the predicted image [10]; Based on the BCS-SPL framework, the sampling rate is set adaptively according to the texture feature of various blocks in [11] and the multi-scale CS theory was addressed in [12]; Additionally, the SPL algorithm using Principal Component Analysis (PCA) was presented for BCS in [13]. To our knowledge, the above methods improved the image reconstruction quality, but with increasing computational complexity and slow convergence, the weakness can be easily observed.

In this paper, we adopt the same basic work of block-based CS sampling of images coupled with SPL-based reconstruction. Our contribution lies in that we cast the reconstruction in the all phase biorthogonal transform (APBT) domain [14], [15] in which the signal has been shown to be sparser than in DCT domain. At the same time, in order to reduce high computational complexity of the SPL-based reconstruction, the semi-iteration [16] skill is enforced to accelerate the convergences of the SPL iteration, called accelerated SPL (ASPL) iteration. In experimental simulations, we find that the proposed BCS-ASPL-APBT reconstruction algorithm outperforms the method using discrete cosine transform (DCT) coupled with the common SPL algorithm and runs faster.

The rest of the paper is organized as follows. Section II provides a brief review of the CS and BCS theory. Section III describes the APBT theory and demonstrates that the signal could be sparser in APBT domain than in DCT domain. Section IV presents the SPL algorithm and Section V proposes the BCS-APBT-ASPL reconstruction algorithm. Section VI reports the simulation results for several typical images followed by conclusions in Section VII.

## II. BACKGROUND

### A. Sparse Representation

Suppose that $\boldsymbol{x} \in R^N$ is a discrete signal that could be represented as a linear combination of the basis $\{\psi_i\}_{i=1}^N$:

$$\boldsymbol{x} = \sum_{i=1}^{N} \theta_i \psi_i = \boldsymbol{\Psi\theta} \tag{1}$$

Manuscript received August 22, 2013; revised April 25, 2014.
This work was supported by the National Natural Science Foundation of China under Grant No. 61002027 and No. 61372145.
Corresponding author email: yangaiping@tju.edu.cn.
doi:10.12720/jcm.9.4.371-378

where $\boldsymbol{\Psi}=[\psi_1,\psi_2,\cdots,\psi_N]$, and $\psi_i$ is a column vector with $\boldsymbol{N}$ elements; $\boldsymbol{\theta}$ is the weight coefficients vector of $\boldsymbol{x}$ : $\theta_i =< \boldsymbol{x},\psi_i >= \psi_i^{-1}\boldsymbol{x}$ . So $\boldsymbol{x}$ and $\boldsymbol{\theta}$ are equivalent representation of the same signal, in the time domain and frequency domain respectively. If the number of non-zero elements $K$ in $\boldsymbol{\theta}$ is far less than $N$ , then $\boldsymbol{x}$ is called $K$ -sparse.

### B. Signal Measurement and Reconstruction

Suppose that we are allowed to take $M$ ($M<<N$) linear, non-adaptive measurements of $\boldsymbol{x}$ through the following linear transformation:

$$\boldsymbol{y} = \boldsymbol{\Phi x} \tag{2}$$

where $\boldsymbol{y}$ represents a $M\times1$ sampling vector and $\boldsymbol{\Phi}$ is a $M\times N$ measurement matrix $\boldsymbol{\Phi}^{M\times N}=\{\phi_1,\phi_2,\cdots,\phi_M\}^{\mathrm{T}}$. Since $M<<N$, the reconstruction of $\boldsymbol{x}$ from $\boldsymbol{y}$ is generally ill-posed. However, the CS theory is based on the fact that the signal $\boldsymbol{x}$ has a sparse representation in $\boldsymbol{\Psi}$ domain. In other words, if the signal is $K$ -sparse and the equivalent sensing matrix $\boldsymbol{\Phi}\cdot\boldsymbol{\Psi}$ satisfies the RIP [3], we can reconstruct $K$ maximum values in $N$-dimensional signal $\boldsymbol{x}$ by $K\log(N/K)$ measurements stably by solving $l_1$ norm optimization:

$$\hat{\boldsymbol{\theta}} = \arg\min\|\boldsymbol{\theta}\|_1 \quad s.t.\ \boldsymbol{y}=\boldsymbol{\Phi\Psi\theta} \tag{3}$$

where $\hat{\boldsymbol{\theta}}$ is the sparse representation vector, thus the signal $\boldsymbol{x}$ can be reconstructed approximately with the transform base $\boldsymbol{\Psi}$ by:

$$\hat{\boldsymbol{x}} = \boldsymbol{\Psi}\hat{\boldsymbol{\theta}} \tag{4}$$

### C. Block Compressed Sensing (BCS)

In BCS [8], the $N\times N$ image $\boldsymbol{x}$ is divided into small blocks with the size of $B\times B$ each and sampled with the same operator. Let $\boldsymbol{x}_j$ ( $j=1,2,\cdots,n$ , $n=(N/B)^2$ ) represents the vectorized signal of the $j$-th block through raster scanning. The corresponding output CS vector $\boldsymbol{y}_j$ can be written as

$$\boldsymbol{y}_j = \boldsymbol{\Phi}_{\mathrm{B}}\boldsymbol{x}_j \tag{5}$$

where $\boldsymbol{\Phi}_{\mathrm{B}}$ is a $n_{\mathrm{B}}\times B^2$ measurement matrix, with $n_{\mathrm{B}}=\lfloor \beta B^2 \rfloor$, $\beta$ is the sampling rate. In our work, $\boldsymbol{\Phi}_{\mathrm{B}}$ is an orthonormalized i.i.d Gaussian matrix [8]. For the whole image, thus the sampling operator $\boldsymbol{\Phi}$ is a block diagonal matrix taking the following form:

$$\boldsymbol{\Phi} = \begin{bmatrix} \boldsymbol{\Phi_B} & & & \\ & \boldsymbol{\Phi_B} & & \\ & & \ddots & \\ & & & \boldsymbol{\Phi_B} \end{bmatrix} \tag{6}$$

Note that BCS is memory efficient as we just need to store a $n_{\mathrm{B}}\times B^2$ Gaussian ensemble $\boldsymbol{\Phi}_{\mathrm{B}}$. Small $B$ requires less memory in storage and faster implementation, while large $B$ offers better reconstruction performance, we choose empirically the block size $B$ = 32 hereafter.

## III. All Phase Biorthogonal Transform (APBT)

### A. All Phase Biorthognal Transform (APBT)

All phase biorthogonal transform (APBT) is derived from all phase sequency filtering (APSF) [14], and the APSF could be completed through the multiplication of a transformation matrix with a desired sequency response vector. The transformation matrix is called all phase biorthogonal transform (APBT) matrix with the properties of reversible, non-orthogonal and good sequency [15]. Different APBT could be posed from different orthogonal transform, such as all phase Walsh biorthogonal transform (APWBT), all phase DCT biorthogonal transform (APDCBT) and all phase IDCT biorthogonal transform (APIDCBT). This article focuses on the latter two, which are usually applicable to the image processing.

Based on the discrete cosine transform sequency filtering, getting the APDCBT matrix

$$T_{\mathrm{APDCBT}}(m,n) = \begin{cases} \dfrac{N-m}{N^2}, & m=0,1,\cdots,N-1,\ n=0 \\ P_1(m,n), & \begin{matrix} m=0,1,\cdots,N-1 \\ n=1,2,\cdots,N-1 \end{matrix} \end{cases} \tag{7}$$

where $P_1(m,n)=\dfrac{1}{N^2}\left[(N-m)\cos\dfrac{mn\pi}{N}-\csc\dfrac{n\pi}{N}\sin\dfrac{mn\pi}{N}\right]$

Accordingly, the APIDCBT matrix is

$$T_{\mathrm{APIDCBT}}(m,n) = \begin{cases} \dfrac{1}{N}, & m=0,\ 0\le n\le N-1 \\ P_2(m,n), & 1\le m\le N-1,\ 0\le n\le N-1 \end{cases} \tag{8}$$

where $P_2(m,n)=\dfrac{N-m+\sqrt{2}-1}{N^2}\cos\dfrac{m(2n+1)\pi}{2N}$.

The APDCBT or APIDCBT matrix $\boldsymbol{T}$ is non-orthogonal, but full rank, with the inverse matrix $\boldsymbol{T^{-1}}$. So the signal could be decomposed using the row vector of the APBT matrix $\boldsymbol{T}$, and reconstructed using the column vector of $\boldsymbol{T^{-1}}$. Fig. 1 illustrates the decomposition basis images and reconstruction basis images of APIDCBT when $N$=8. Like DCT, the two-dimensional sequency of the decomposition basis images and the reconstruction basis images of APBT increase from the upper left to the lower right. So the column and row vectors of the APBT matrix have good sequency properties and could be used in sequency analysis and synthesis of the signal, and APBT could decorrelate the signal effectively.

It can be demonstrated that the energy of the decomposition basis images of the APBT [14] decreases gradually with the increase of the sequency in the direction of the main diagonal, while that of the reconstruction basis images of the APBT increases. So

the APBT coefficients have good high-frequency attenuation, more applicable to the spectrum distribution of the natural signal than DCT.

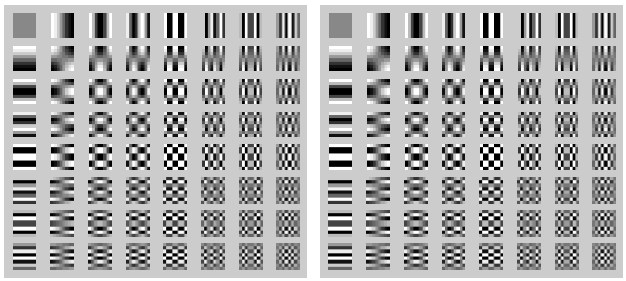

Fig. 1. The basis images of APIDCBT. Left: Decompsition basis images, right: Reconstruction basis images

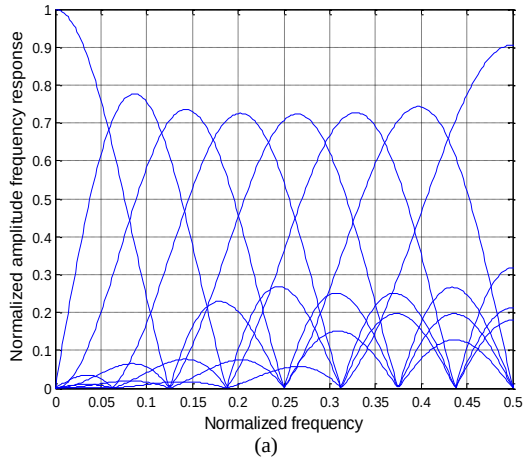


Fig. 2. The frequency response of the filters in: (a) DCT, (b) APIDCBT

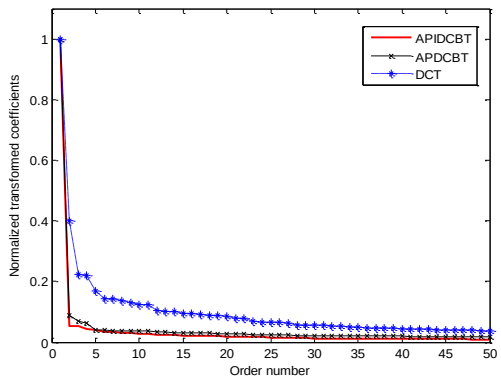


Fig. 3. The sorted transformed coefficients

In addition, Fig. 2 illustrates the normalized amplitude-frequency response of the filters in DCT and APBT. It can be seen that APBT reveals the sparsity better by giving more emphasis to the low-frequency band than that of DCT. For example, the DCT and APBT coefficients of the 64×64 typical image 'Lena' are sorted in descending order and the first 50 are plotted in Fig. 3. It can be shown that the distribution curves of APBT have a better attenuation than that of DCT, and that of APIDCBT is the steepest.

### *B. Transform and Inverse Transform of APBT*

As mentioned above, the APBT matrix $\boldsymbol{T}$ is non-orthogonal, i.e. $\boldsymbol{T}^{\mathrm{T}} \neq \boldsymbol{T}^{-1}$. Similar to the biorthogonal wavelet transform, two different bases need to be used in operating the signal decomposition and reconstruction. Here let $\boldsymbol{T}$ denoting the decomposition matrix and $\boldsymbol{T}^{-1}$ denoting the reconstruction matrix. For the 2-D image $\boldsymbol{x}$, the decomposition of the image is as follows

$$\boldsymbol{Y}=\boldsymbol{T}\boldsymbol{X}\boldsymbol{T}^{\mathrm{T}} \tag{9}$$

So the reconstruction of $\boldsymbol{X}$ based on the transformed coefficient matrix $Y$ is as follows

$$\boldsymbol{X}=\boldsymbol{T}^{-1}\boldsymbol{Y}(\boldsymbol{T}^{-1})^{\mathrm{T}} \tag{10}$$

## IV. Projected Landweber (PL) Iteration

The standard Landweber iteration is:

$$\boldsymbol{x}^{[k+1]}=\boldsymbol{x}^{[k]}+\omega\boldsymbol{\Phi}^{T}(\boldsymbol{y}-\boldsymbol{\Phi}\boldsymbol{x}^{[k]}) \tag{11}$$

where $\omega$ $(0<\omega\leq 1/\|\boldsymbol{\Phi}\|^{2})$ is a relaxation parameter to control the iterative process. The projected Landweber (PL) is based on the prior information of the original image which can be expressed in some closed convex sets [17]. The PL algorithm could be written as:

$$\boldsymbol{x}^{[k+1]}=\mathrm{P}_{C}\left[\boldsymbol{x}^{[k]}+\omega\boldsymbol{\Phi}^{T}(\boldsymbol{y}-\boldsymbol{\Phi}\boldsymbol{x}^{[k]})\right] \tag{12}$$

where $P_C$ is a operator projecting a vector in $[\cdot]$ to the closed convex set C. The classical form of this kind algorithm usually includes: Landweber iteration, projection and thresholding; for example, the CS reconstruction based on PL iteration in [18] including the following steps, starts from some initial approximation $\boldsymbol{x}^{[0]}$:

1) Landwever iteration:

$$\hat{\boldsymbol{x}}^{[k]}=\boldsymbol{x}^{[k]}+\omega\boldsymbol{\Phi}^{T}(\boldsymbol{y}-\boldsymbol{\Phi}\boldsymbol{x}^{[k]})$$

2) Projecting and thresholding:

$$\hat{\boldsymbol{\theta}}^{[k]}=\boldsymbol{\Psi}\hat{\boldsymbol{x}}^{[k]},\ \tilde{\boldsymbol{\theta}}^{[k]}=\mathrm{Threshold}(\hat{\boldsymbol{\theta}}^{[k]},\lambda)$$

3) Reconstruction through the inverse transform:

$$\boldsymbol{x}^{[k+1]}=\boldsymbol{\Psi}^{-1}\tilde{\boldsymbol{\theta}}^{[k]}$$

where $\boldsymbol{\Phi}$ is the measurement matrix, $\boldsymbol{\Psi}$ is the transform matrix, i.e., the projecting matrix; Threshold(·) is a hard thresholding operator owning the larger elements than

$\tau = \lambda\sigma\sqrt{2\log m}$ and setting the others to zero in $\hat{\boldsymbol{\theta}}^{[k]}$, here $\tau$ is decided by $\lambda$ that is a constant controlling the convergence and $\sigma$ is estimated noise standard deviation, $m$ is the number of the transform coefficients [19].

Like the greedy algorithms of the pursuits class, the projected Landweber based CS reconstruction also provides reduced computational complexity. Additionally, the PL formulation offers the possibility of easily enforcing additional optimization criteria. For example, the smoothing based on Wiener filtering was imposed to the PL framework namely smoothed PL (SPL) in [9]. However, the PL step still needs a large number of iteration especially being applied to the image CS reconstruction. So the accelerated Landweber formulation is proposed in the next section and the thresholding is operated in the APBT domain at the same time.

## V. ASPL-APBT BASED IMAGE BCS RECONSTRUCTION

### A. Accelerated Landweber Iteration

The main drawback of Landweber iteration in (7) is its slow rate of convergence, it constructs a new approximation vector $\boldsymbol{x}^{[k]}$ with the previous iteration $\boldsymbol{x}^{[k-1]}$ only, and the relaxation parameter $\omega$ is difficult to choose. To overcome these drawbacks, the so-called semi-iterative method was proposed in [16]. The semi-iterative based methods have been known as the polynomial acceleration technique, and the basic idea of semi-iterative method consists of one step of iteration, followed by an averaging process over all or some of the previously obtained approximations. The iterative step has the form:

$$\begin{aligned}\boldsymbol{x}^{[k]} = \mu_{1,k}\boldsymbol{x}^{[k-1]} + \mu_{2,k}\boldsymbol{x}^{[k-2]} + \cdots + \\ \mu_{k,k}\boldsymbol{x}^{[0]} + \omega_k\boldsymbol{\Phi}^{\mathrm{T}}(\boldsymbol{y} - \boldsymbol{\Phi}\boldsymbol{x}^{[k-1]})\end{aligned} \tag{13}$$

where,

$$\sum_{i=1}^{k}\mu_{i,k} = 1,\ \omega_k \neq 0, k \geq 1 \tag{14}$$

Obviously, the Landweber iteration is a special case of (13), when $\omega_k = \omega$, $\mu_{1,k} = \mu_{2,k} = \cdots = \mu_{k,k} = 0$ in (11).

With the purpose of avoiding the overburden memory, here we just use the information of a few steps in (13). Additionally, in order to reach the optimal rate of convergence, we use the $\gamma$-method when determining the parameters in (13) [16]. Specifically,

$$\boldsymbol{x}^{[k]} = \boldsymbol{x}^{[k-1]} + \mu_k(\boldsymbol{x}^{[k-1]} - \boldsymbol{x}^{[k-2]}) + \omega_k\boldsymbol{\Phi}^{\mathrm{T}}(\boldsymbol{y} - \boldsymbol{\Phi}\boldsymbol{x}^{[k-1]}) \tag{15}$$

where,

$$\mu_1 = 0,\ \omega_1 = \frac{4\gamma + 2}{4\gamma + 1} \tag{16}$$

$$\mu_k = \frac{(k-1)(2k-3)(2k+2\gamma-1)}{(k+2\gamma-1)(2k+4\gamma-1)(2k+2\gamma-3)} \tag{17}$$

$$\omega_k = \frac{4(2k+2\gamma-1)(k+\gamma-1)}{(k+2\gamma-1)(2k+4\gamma-1)} \tag{18}$$

The $\gamma$-method takes the linear combination of the current negative gradient $\boldsymbol{\Phi}^{\mathrm{T}}(\boldsymbol{y} - \boldsymbol{\Phi}\boldsymbol{x}^{[k-1]})$ and the searches the direction of the previous step $(\boldsymbol{x}^{[k-1]} - \boldsymbol{x}^{[k-2]})$ as the new search direction, which is non-orthogonal to the gradient direction so as to avoid the zigzagging toward solution.

### B. ASPL-APBT based BCS Image Reconstruction

As mentioned above, the PL iteration has been applied in BCS reconstruction [8], [9], and several prominent directional transforms are incorporated into the PL formulation to improve the sparsity of the image [9]. However, these directional transforms couldn't be applicable to the blocked image and commonly have not fast algorithms. Therefore, we select the APBT which are suitable to the blocked image with better sparsifying than common used DCT and it can be shown that better reconstructed results could be obtained than using the wavelet transform in several experiments.

Additionally, in order to speed up the convergence in BCS reconstruction of the image, the accelerated Landweber iteration is adopted. At the same time the smoothing step using Wiener-filtering is interleaved with the accelerated PL iteration, we called the accelerated smoothed PL (ASPL). So the ASPL-APBT based BCS image reconstruction algorithm is proposed. The following are the specific steps, and $\boldsymbol{\Psi}$, $\boldsymbol{\Psi}^{-1}$ represent the APBT and its inverse transform operator respectively.

**Input**: the measurement vector $\boldsymbol{y}$, orthonormalized i.i.d Gaussian matrix $\boldsymbol{\Phi}_{\mathrm{B}}$, thresholding parameter $\lambda$;

**Initialization**: **letting** $\boldsymbol{x}^{[0]} = \boldsymbol{\Phi}_B^{\mathrm{T}}\boldsymbol{y}$ and getting $\hat{\boldsymbol{x}}^{[0]}$ after Wiener filtering; error tolerance $\varepsilon > 0$; maximum number of iteration $k_{\max}$, and letting $k = 0$;

**Solving** $\boldsymbol{x}^{[1]}$: **using** (15) and (16) to get $\bar{\boldsymbol{x}}^{[1]}$, and $\boldsymbol{\theta}^{[1]} = \boldsymbol{\Psi}\boldsymbol{x}^{[1]}$, $\tilde{\boldsymbol{\theta}}^{[1]} = \mathrm{Threshold}(\boldsymbol{\theta}^{[1]}, \lambda)$, $\boldsymbol{x}^{[1]} = \boldsymbol{\Psi}^{-1}\tilde{\boldsymbol{\theta}}^{[1]}$.

**Iteration steps**: $k = k+1$, if $|\boldsymbol{D}^{[k+1]}\text{-}\boldsymbol{D}^{[k]}| > \varepsilon$ or $k < k_{\max}$, do the following steps:

- Smoothing operating $\hat{\boldsymbol{x}}^{[k]}$ =Wiener ( $\boldsymbol{x}^{[k]}$);
- Computing parameters $\mu_k$, $\omega_k$ using (17) and (18);
- For each image block, computing accelerated Landweber iteration:

$$\hat{\hat{\boldsymbol{x}}}_j^{[k+1]} = \hat{\boldsymbol{x}}_j^{[k]} + \mu_{k+1}(\hat{\boldsymbol{x}}_j^{[k]} - \hat{\boldsymbol{x}}_j^{[k-1]}) + \omega_{k+1}\boldsymbol{\Phi}_B^{\mathrm{T}}(\boldsymbol{y}_j\text{-}\boldsymbol{\Phi}_B\hat{\boldsymbol{x}}_j^{[k]});$$

- Projecting and thresholding:

$$\boldsymbol{\theta}^{[k+1]} = \boldsymbol{\Psi}\hat{\hat{\boldsymbol{x}}}^{[k+1]};\ \tilde{\boldsymbol{\theta}}^{[k+1]} = \mathrm{Threshold}(\boldsymbol{\theta}^{[k+1]}, \lambda);$$

- Reconstruction through inverse transform:

$$\bar{\boldsymbol{x}}^{[k+1]} = \boldsymbol{\psi}^{-1}\tilde{\boldsymbol{\theta}}^{[k+1]};$$

- Letting $x^{[k]} = \bar{x}^{[k+1]}$, $x^{[k-1]} = \hat{x}^{[k]}$, again accelerated Landweber iteration for each block $j$:
  $\boldsymbol{x}_j^{[k+1]} = \boldsymbol{x}_j^{[k]} + \mu_{k+1}(\boldsymbol{x}_j^{[k]} - \boldsymbol{x}_j^{[k-1]}) + \omega_{k+1}\boldsymbol{\Phi}_B^{\mathrm{T}}(\boldsymbol{y}_j - \boldsymbol{\Phi}_B \boldsymbol{x}_j^{[k]})$;
  **Output**: Reconstructed image $x$.

Here, Wiener $(\cdot)$ is pixel wise adaptive Wiener filtering using a neighborhood of 3×3, Threshold$(\bullet)$ is the hard thresholding operator with the same definition discussed in section 4. The termination rule is $|\boldsymbol{D}^{[k+1]} - \boldsymbol{D}^{[k]}| < \varepsilon$, where $\varepsilon$ is the error tolerance, and $\boldsymbol{D}^{[k]} = \left\| \boldsymbol{x}^{[k+1]} - \hat{\boldsymbol{x}}^{[k]} \right\| / \sqrt{N}$.

TABLE I. PSNR RESULTS

| Algorithm (PSNR/dB) | Measurement Rate (*M/N*) | | | | |
|---|---|---|---|---|---|
| | 0.1 | 0.2 | 0.3 | 0.4 | 0.5 |
| **Lena** | | | | | |
| BCS-SPL-DCT | 27.70 | 30.45 | 32.46 | 34.19 | 35.77 |
| BCS-SPL-APDCBT | 28.10 | 31.11 | 33.20 | 34.96 | 36.54 |
| BCS-SPL-APIDCBT | 28.12 | 31.15 | 33.27 | 35.03 | 36.61 |
| BCS-ASPL-DCT | 27.72 | 30.51 | 32.55 | 34.26 | 35.92 |
| BCS-ASPL-APDCBT | 28.12 | 31.17 | 33.30 | 35.10 | 36.68 |
| BCS-ASPL-APIDCBT | **28.13** | **31.23** | **33.37** | **35.15** | **36.76** |
| **Barbara** | | | | | |
| BCS-SPL-DCT | 22.76 | 24.38 | 25.91 | 27.42 | 29.05 |
| BCS-SPL-APDCBT | 22.63 | 23.98 | 25.44 | 27.22 | 28.99 |
| BCS-SPL-APIDCBT | 22.65 | 24.00 | 25.48 | 27.25 | 29.09 |
| BCS-ASPL-DCT | **22.88** | **24.49** | **25.80** | 27.53 | 29.09 |
| BCS-ASPL-APDCBT | 22.68 | 24.18 | 25.74 | 27.55 | 29.39 |
| BCS-ASPL-APIDCBT | 22.69 | 24.19 | 25.77 | **27.58** | **29.41** |
| **Goldhill** | | | | | |
| BCS-SPL-DCT | 26.10 | 28.32 | 29.63 | 30.98 | 32.57 |
| BCS-SPL-APDCBT | 26.95 | 29.07 | 30.69 | 32.15 | 33.49 |
| BCS-SPL-APIDCBT | 26.96 | 29.08 | 30.72 | 32.18 | 33.59 |
| BCS-ASPL-DCT | 26.54 | 28.70 | 30.32 | 31.67 | 33.15 |
| BCS-ASPL-APDCBT | 26.97 | 29.22 | 30.84 | 32.30 | 33.69 |
| BCS-ASPL-APIDCBT | **26.99** | **29.24** | **30.87** | **32.34** | **33.72** |
| **Peppers** | | | | | |
| BCS-SPL-DCT | 27.49 | 30.60 | 32.37 | 33.76 | 35.01 |
| BCS-SPL-APDCBT | 28.24 | 31.40 | 33.22 | 34.61 | 35.83 |
| BCS-SPL-APIDCBT | 28.34 | 31.45 | 33.32 | 34.67 | 35.93 |
| BCS-ASPL-DCT | 27.94 | 31.21 | 33.08 | 34.48 | 35.78 |
| BCS-ASPL-APDCBT | 28.37 | 31.60 | 33.37 | 34.72 | 35.92 |
| BCS-ASPL-APIDCBT | **28.43** | **31.65** | **33.45** | **34.78** | **35.99** |
| **Mandrill** | | | | | |
| BCS-SPL-DCT | 20.24 | 21.31 | 22.31 | 23.40 | 24.51 |
| BCS-SPL-APDCBT | 20.54 | 21.76 | 22.87 | 23.98 | 25.14 |
| BCS-SPL-APIDCBT | 20.54 | 21.78 | 22.90 | 24.04 | 25.19 |
| BCS-ASPL-DCT | 20.32 | 21.54 | 22.59 | 23.69 | 24.86 |
| BCS-ASPL-APDCBT | 20.55 | 21.77 | 22.91 | 24.04 | 25.22 |
| BCS-ASPL-APIDCBT | **20.56** | **21.79** | **22.93** | **24.08** | **25.27** |

## VI. EXPERIMENTAL RESULTS

To evaluate the proposed ASPL-APBT based BCS image reconstruction algorithm, comprehensive experiments were carried out using Matlab R2012b on a 2.80GHz processors and 2GB memory computer.

### A. The Quality of Reconstructed Image

Firstly, to evaluate the effectiveness of the increased sparsity of the APBT in representing the image and the performance of the ASPL in BCS reconstruction, we employ the DCT, APDCBT and APIDCBT within the SPL and ASPL framework respectively. We refer to the resulting implementations as BCS-SPL-DCT, BCS-SPL-APDCBT and BCS-SPL-APIDCBT, BCS-ASPL-DCT, BCS-ASPL-APDCBT and BCS-ASPL-APIDCBT. According to the experimental results, in the SPL framework, we use hard thresholding with $\lambda$ =6, 10, and 10, correspondingly, for BCS-SPL-DCT, BCS-SPL-APDCBT and BCS-SPL-APIDCBT; In ASPL framework, we use hard thresholding with $\lambda$ =2, 4, and 4, correspondingly, for BCS-ASPL-DCT, BCS-ASPL-APDCBT and BCS-ASPL-APIDCBT.

Table I compares PSNR for five 512×512 images Lena, Barbara, Goldhill, Peppers and Mandrill at several measurement ratios. Noting that the quality of reconstruction can vary due to the randomness of the measurement matrix $\boldsymbol{\Phi}_B$, all PSNRs are averaged over 5 independent trials.

As shown in Table I, the PSNR results of BCS-SPL and BCS-ASPL based on APBT yield about 0.4-1.2dB improvement, respectively, compared to BCS-SPL and BCS-ASPL based on DCT except Barbara; The ASPL based results outperform SPL based whether in APBT domain or DCT domain. For APDCBT and APDCBT, the PSNR results are roughly the same. The PSNR of ASPL based algorithms have more improvements than SPL based on DCT, especially for Goldhill, Peppers and Mandrill, and maximum up to 0.86dB improvement.

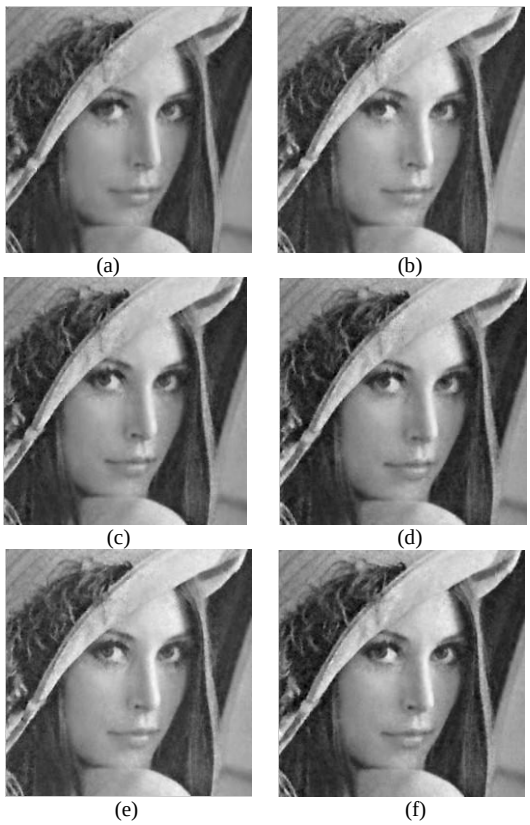


Fig. 4. Lena for *M/N* = 20%. (a) BCS-SPL-DCT, (b) BCS-SPL-APDCBT, (c) BCS-SPL-APIDCBT, (d) BCS-ASPL-DCT, (e) BCS-ASPL-APDCBT, (f) BCS-ASPL-APIDCBT

Fig. 4 illustrates example visual results. It could be shown that the APBT based reconstruction provides better quality than the DCT based techniques both within BCS-SPL and BCS-ASPL framework. Especially the BCS-ASPL based algorithms are more desirable.

TABLE II. RUNNING TIME

| Algorithm (Running time/s) | Measurement Rate (*M/N*) | | | | |
|---|---|---|---|---|---|
| | 0.1 | 0.2 | 0.3 | 0.4 | 0.5 |
| **Lena** | | | | | |
| BCS-SPL-DCT | 43.1 | 35.2 | 30.1 | 28.6 | 24.4 |
| BCS-SPL-APDCBT | 80.2 | 56.8 | 49.3 | 46.4 | 36.5 |
| BCS-SPL-APIDCBT | 83.8 | 57.9 | 49.5 | 46.4 | 38.5 |
| BCS-ASPL-DCT | 15.6 | 12.4 | 11.5 | 10.7 | 10.3 |
| BCS-ASPL-APDCBT | 27.8 | 18.9 | 17.8 | 15.9 | 16.9 |
| BCS-ASPL-APIDCBT | 30.1 | 23.3 | 19.7 | 17.7 | 17.8 |
| **Barbara** | | | | | |
| BCS-SPL-DCT | 43.7 | 34.9 | 31.8 | 29.0 | 27.9 |
| BCS-SPL-APDCBT | 76.8 | 62.1 | 48.5 | 47.6 | 43.1 |
| BCS-SPL-APIDCBT | 81.2 | 62.6 | 52.6 | 50.9 | 48.4 |
| BCS-ASPL-DCT | 14.2 | 12.3 | 11.4 | 10.9 | 10.3 |
| BCS-ASPL-APDCBT | 29.4 | 23.6 | 19.6 | 18.1 | 17.5 |
| BCS-ASPL-APIDCBT | 32.9 | 19.5 | 18.3 | 17.9 | 17.2 |
| **Goldhill** | | | | | |
| BCS-SPL-DCT | 43.6 | 30.8 | 28.3 | 25.1 | 23.1 |
| BCS-SPL-APDCBT | 78.4 | 56.6 | 48.9 | 42.5 | 39.3 |
| BCS-SPL-APIDCBT | 86.8 | 56.9 | 49.5 | 42.6 | 39.3 |
| BCS-ASPL-DCT | 14.7 | 12.5 | 11.4 | 9.8 | 9.9 |
| BCS-ASPL-APDCBT | 38.9 | 19.7 | 20.2 | 18.6 | 16.7 |
| BCS-ASPL-APIDCBT | 29.0 | 19.3 | 21.1 | 18.1 | 16.7 |
| **Peppers** | | | | | |
| BCS-SPL-DCT | 20.8 | 19.4 | 17.2 | 16.1 | 13.8 |
| BCS-SPL-APDCBT | 32.5 | 24.1 | 22.8 | 20.2 | 19.5 |
| BCS-SPL-APIDCBT | 35.8 | 25.4 | 23.6 | 20.9 | 19.5 |
| BCS-ASPL-DCT | 14.0 | 12.8 | 11.6 | 10.9 | 10.4 |
| BCS-ASPL-APDCBT | 26.8 | 21.7 | 16.8 | 15.9 | 15.2 |
| BCS-ASPL-APIDCBT | 28.4 | 21.8 | 18.5 | 17.3 | 15.3 |
| **Mandrill** | | | | | |
| BCS-SPL-DCT | 20.8 | 19.4 | 17.2 | 16.1 | 13.8 |
| BCS-SPL-APDCBT | 32.5 | 24.1 | 22.8 | 20.2 | 19.5 |
| BCS-SPL-APIDCBT | 35.8 | 25.4 | 23.6 | 20.9 | 19.5 |
| BCS-ASPL-DCT | 14.0 | 12.8 | 11.6 | 10.9 | 10.4 |
| BCS-ASPL-APDCBT | 26.8 | 21.7 | 16.8 | 15.9 | 15.2 |
| BCS-ASPL-APIDCBT | 28.4 | 21.8 | 18.5 | 17.3 | 15.3 |

## B. Running Time

Table II compares the reconstruction time for the reconstructed image at several measurement ratios. The results are averaged over independent trials. Fig. 5 illustrates the distribution curves of running time for Lena and Goldhill. It can be shown from Table II and Fig. 5 that the running time in ASPL based framework is shorter than that of the SPL based. The APBT based run more time than DCT based, in that APBT based algorithms need calculating inverse matrix but not the transpose matrix like in DCT. But the difference tends to be less with the increase of measurement rate.

## C. Number of Iterations

Table III illustrates the number of iterations at several measurement ratios; Fig. 6 illustrates the corresponding curves of Lena and Goldhill. It can be shown that the iteration number of ASPL based algorithms reduce a lot than SPL based. The iteration numbers of APBT based algorithms are much less than DCT based and the iteration number of ASPL based algorithms are roughly the same.

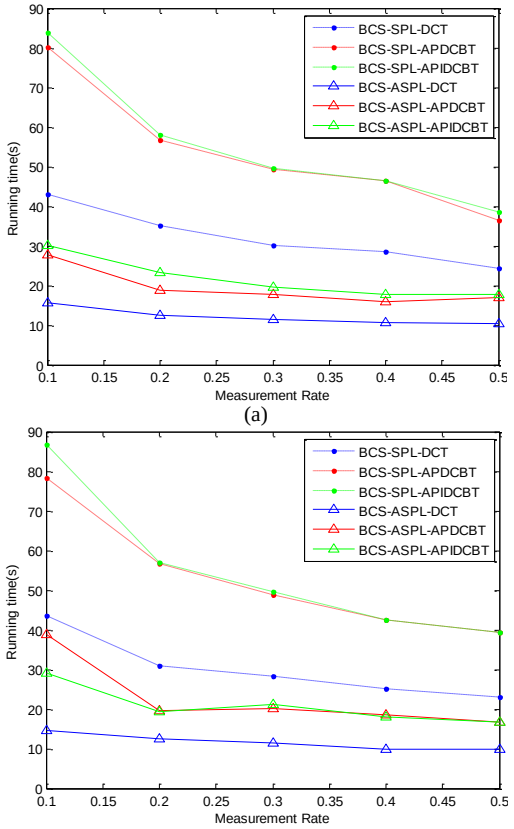


Fig. 5. Running time of (a) Lena, (b) Goldhill

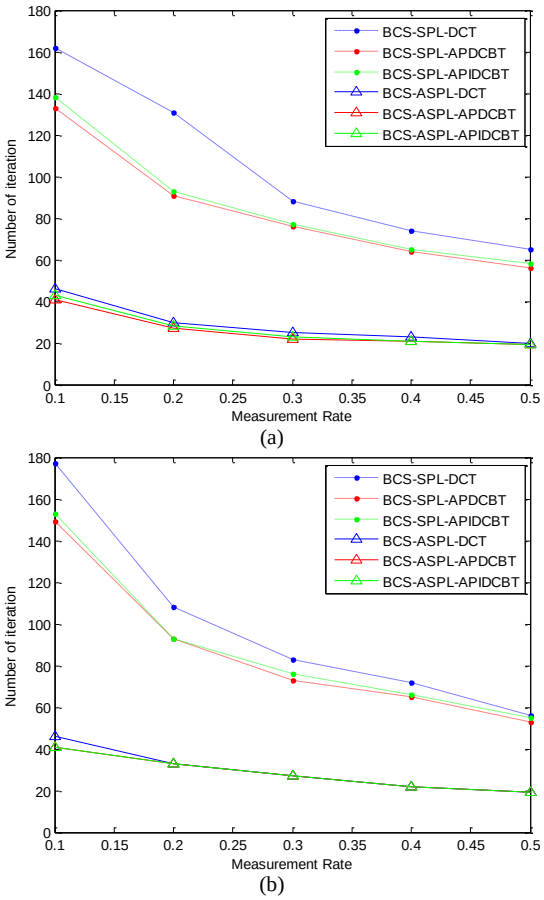


Fig. 6. Number of iterations of (a) Lena, (b) Goldhill

TABLE III. NUMBER OF ITERATION

| Algorithm (Number of iteration) | Measurement Rate (*M/N*) | | | | |
|---|---|---|---|---|---|
| | 0.1 | 0.2 | 0.3 | 0.4 | 0.5 |
| **Lena** | | | | | |
| BCS-SPL-DCT | 162 | 131 | 88 | 74 | 65 |
| BCS-SPL-APDCBT | 133 | 91 | 76 | 64 | 56 |
| BCS-SPL-APIDCBT | 138 | 93 | 77 | 65 | 58 |
| BCS-ASPL-DCT | 46 | 30 | 25 | 23 | 20 |
| BCS-ASPL-APDCBT | 41 | 27 | 22 | 21 | 19 |
| BCS-ASPL-APIDCBT | 43 | 28 | 23 | 21 | 19 |
| **Barbara** | | | | | |
| BCS-SPL-DCT | 164 | 121 | 89 | 74 | 66 |
| BCS-SPL-APDCBT | 143 | 102 | 78 | 64 | 58 |
| BCS-SPL-APIDCBT | 145 | 104 | 79 | 65 | 62 |
| BCS-ASPL-DCT | 46 | 32 | 27 | 23 | 16 |
| BCS-ASPL-APDCBT | 44 | 29 | 23 | 21 | 15 |
| BCS-ASPL-APIDCBT | 45 | 27 | 24 | 22 | 15 |
| **Goldhill** | | | | | |
| BCS-SPL-DCT | 177 | 108 | 83 | 72 | 56 |
| BCS-SPL-APDCBT | 149 | 93 | 73 | 65 | 53 |
| BCS-SPL-APIDCBT | 153 | 93 | 76 | 66 | 55 |
| BCS-ASPL-DCT | 46 | 33 | 27 | 22 | 19 |
| BCS-ASPL-APDCBT | 41 | 33 | 27 | 22 | 19 |
| BCS-ASPL-APIDCBT | 44 | 33 | 28 | 22 | 19 |
| **Peppers** | | | | | |
| BCS-SPL-DCT | 73 | 60 | 47 | 39 | 33 |
| BCS-SPL-APDCBT | 56 | 37 | 30 | 27 | 24 |
| BCS-SPL-APIDCBT | 58 | 40 | 32 | 28 | 25 |
| BCS-ASPL-DCT | 46 | 35 | 28 | 22 | 20 |
| BCS-ASPL-APDCBT | 41 | 29 | 23 | 20 | 17 |
| BCS-ASPL-APIDCBT | 45 | 30 | 23 | 21 | 18 |
| **Mandrill** | | | | | |
| BCS-SPL-DCT | 73 | 60 | 47 | 39 | 33 |
| BCS-SPL-APDCBT | 56 | 37 | 30 | 27 | 24 |
| BCS-SPL-APIDCBT | 58 | 40 | 32 | 28 | 25 |
| BCS-ASPL-DCT | 46 | 35 | 28 | 22 | 20 |
| BCS-ASPL-APDCBT | 41 | 29 | 23 | 20 | 17 |
| BCS-ASPL-APIDCBT | 45 | 30 | 23 | 21 | 18 |

## VII. CONCLUSIONS

In this paper, we examined the use of APBT in the CS reconstruction of images. We adopted the general paradigm of block-based random image sampling coupled with a projection-based accelerated Landweber reconstruction not only promoting the sparsity and smoothness of the reconstruction, but also speeding up the convergence. The proposed BCS-ASPL-APBT algorithms outperform not only in reconstruction quality but also in running time and number of iterations.

## ACKNOWLEDGMENT

This work was supported by the National Natural Science Foundation of China (Grant No. 61002027, 61372145). The authors would like to thank Xiaoyan Fu for her help and valuable suggestions to improve the presentation of the paper.

## REFERENCES

[1] E. J. Candés, J. Romberg, and T. Tao, "Robust uncertainty principles: Exact signal reconstruction from highly incomplete frequency information," *IEEE Trans. on Information Theory*, vol.52, no.2, pp. 489-509, Feb. 2006.

[2] D. L. Donoho, "Compressed sensing," *IEEE Trans. on Information Theory*, vol.52, no. 4, pp. 1289-1306, July 2006.

[3] G. M. Shi, D. H. Liu, D. H. Gao, Z. Liu, J. Lin, *et al.*, "Advances in theory and application of compressed sensing," *Journal of electronics*, vol. 37, no. 5, pp. 1070-1081, May 2009.

[4] M. A. T. Figueiredo, R. D. Nowak, and S. J. Wright, "Gradient projection for sparse reconstruction: Application to compressed sensing and other inverse problems," *IEEE Journal on Selected Areas in Communications*, vol. 1, no. 4, pp. 586–597, Dec. 2007.

[5] T. T. Do, L. Gan, N. Nguyen, and T. D. Tran, "Sparsity adaptive matching pursuit algorithm for practical compressed sensing," in *Proc. 42th Asilomar Conference on Signals, Systems, and Computers*, Pacific Grove, California, Oct. 2008, pp. 581–587.

[6] T. Do, L. Gan, and N. Nguyen, "Fast and efficient compressive sensing using structurally random matrices," *IEEE Trans. on Signal Processing*, vol. 60, no. 1, pp. 139-154, 2012.

[7] L. Gan, T. Do, and T. D. Tran, "Fast compressive imaging using scrambled block Hadamard ensemble," in *Proc. European Signal Processing Conference*, Lausannne, Switzerland, Aug. 2008, pp. 1-5.

[8] L. Gan, "Block compressed sensing of natural images," presented at proceedings of the International Conference on Digital Signal Processing, Cardiff, UK, July 2007, pp. 403–406.

[9] S. Mun and J. E. Fowler, "Block compressed sensing of images using directional transforms," presented at proceedings of the International Conference on Image Processing, Cairo, Egypt, Nov.

2009, pp. 3021-3024.
[10] C. Chen, E. W. Tramel, and J. E. Fowler, "Compressed-sensing recovery of images and video using multihypothesis predictions," presented at proceeding of the 45th Asilomar Conference on Signal, Systems and Computers, Pacific Grove, CA, Nov. 2011, pp. 1193-1198.
[11] A.-H. Wang, L. Liu, B. Zeng, and H.-H. Bai, "Progressive image coding based on an adaptive block compressed sensing," *IEICE Electronics Express*, vol. 8, no. 8, pp. 575-581, April 2011.
[12] J. E. Fowler, S. Mun, and E. W. Tramel, "Multiscale block compressed sensing with smoothed projected landweber reconstruction," presented at proceedings of the European Signal Processing Conference, Barcelona, Spain, 2011, pp. 564-568.
[13] R. Li, Z.-L. Gan, and X.-C. Zhu, "Smoothed projected image compressed sensing reconstruction using hard thresholding based on principal components analysis," *Journal of Image and Graphics*, vol. 18, no. 5, pp. 504-514, Jan.2013.
[14] Z.-X. Hou, "Design and application of the discrent cosine sequency filters," *Journal of Tianjin university*, vol. 32, no. 3, pp. 324-328, May 1999.
[15] Z.-X. Hou, C.-Y. Wang and A.-P. Yang, "All phase biorthogonal transform and its application in JPEG-like image compression," *Signal Processing: Image Communication*, vol. 24, no. 10, pp. 791-802, Nov. 2009.
[16] M. Hanke, "Accelerated Landweber iterations for the solution of ill-posed equations," *Numerische Mathematik*, vol. 60, no. 3, pp. 341–373, 1991.
[17] E. J. Candés and J. Romberg. (2005). Practical signal recovery from random projections. [Online]. Available: http://www.dsp.ece.rice.edu/CS/
[18] J. Haupt and R. Nowak, "Signal reconstruction from noisy random projections," *IEEE Trans. on Information Theory*, vol. 52, no. 9, pp. 4036–4048, Sep. 2006.
[19] D. L. Donoho, "De-noising by soft thresholding," *IEEE Trans. on Information Theory*, vol. 41, no. 3, pp. 613–627, May 1995.

**Aiping Yang** received her B.Ed. degree in mathematics education from Shandong Normal University, China, in 2000 and her M.S. degree in operations research and control theory from Tianjin University, China, in 2003 and her Ph.D. degree in signal and information processing from Tianjin University, China, in 2008. Now she is an associate professor in Tianjin University, China. Her current research interests include digital image and video processing, compressive sensing theory, and wavelet analysis.

**Gai Li** received her bachelor's degree in electronic and information engineering from Henan Normal University, China, in 2011. Now she is a postgraduate student in school of electronic and information engineering, Tianjin University, China. Her current research interest is compressed sensing reconstruction.

**Zhengxin Hou** received the B.E. degree in electrical engineering from Peking University, China, in 1969 and the M.E. degree from Tianjin University, China,in 1982. Now he is a professor and supervisor of the Ph.D. students in Tianjin University, China. His current research interests include compressed sensing, digital signal processing, and wavelet analysis.